RSC Advances

PAPER

View Article Online
View Journal | View Issue

Cite this: *RSC Adv.*, 2024, **14**, 15856

Ni-based catalysts supported on Hbeta zeolite for the hydrocracking of waste polyolefins†

Guoqing Zhang,[a] Qingguo Mao,[b] Yiqun Yue,[a] Ruitong Gao,[a] Yajing Duan[c] and Hui Du *[a]

Polyolefin plastics are the most popular polymer materials worldwide, and the catalytic degradation of post-consumer polyolefins has attracted increased attention as a viable process. In this study, two types of Ni-based catalysts supported on Hbeta zeolite, Ni-Hbeta and NiS_2-Hbeta, have been successfully synthesized for the hydrocracking of waste polyolefin. The experimental results indicated that the synergistic effect between Ni or NiS_2 and the acidic sites of Hbeta zeolites can significantly enhance the tandem cracking and hydrogenation of polyolefin plastics, which suppresses the formation of gas products and coke. Ni-Hbeta employed as a catalyst can effectively degrade HDPE into high value liquid and gas products with high yield of 94% under 523 K and 3 MPa H_2, while also exhibiting excellent cycle stability. In particular, Ni-Hbeta shows better catalytic performance than NiS_2-Hbeta during the hydrocracking of HDPE at a relatively low temperature of 523 K. Furthermore, Ni-Hbeta catalyst also exhibits a remarkable capability for efficient depolymerization of unsorted post-consumer polyolefin plastics (HDPE, LDPE, PP) containing various additives and pollutants. These findings underscore the application potential of employing noble metal-free and recyclable catalysts for hydrocracking plastic waste, thereby facilitating the realization of a circular economy for plastics.

Received 16th April 2024
Accepted 9th May 2024

DOI: 10.1039/d4ra02809k

rsc.li/rsc-advances

Introduction

Around 10 billion tons of plastic have been produced globally since the advent of plastics.[1] Unfortunately, only ~9% of the post-consumed plastics have been recycled,[2] while the remainder has been incinerated, discarded in landfills, or released into the natural environment.[3] There has been a substantial accumulation of plastic waste in the environment, posing threats to both human health and the natural ecosystem, as well as resulting in significant resource waste.[4–6] To solve these aforementioned issues, a new plastic circular economy model is desperately needed to replace the conventional linear economic model.[7,8] This new circular model will enable the closed-loop recycling and upcycling of plastics, contributing to resolve the pressing issue of plastic pollution.[9,10]

Nowadays, polyolefin plastics are the most popular polymer materials worldwide, owing to their exceptional qualities such as high chemical inertness, corrosion resistance, and insulation properties.[11] The life cycle of polyolefin plastics is shortening due to the growing demand and quality requirements for polyolefin plastics in agriculture, packaging, and daily necessities. Despite the growing demand for the recycling of polyolefin plastic, only a small percent of high-purity polyolefin plastics are commercially available for mechanical recycling due to the constraints of purity and cost.[12] Moreover, recycled plastics produced through mechanical recycling can only be downgraded for use due to polymer degradation, product contamination and other issues.[13] In contrast, chemical recycling, an ideal recycling or even upcycling process that can convert polyolefin plastics into hydrocarbon fuels, lubricants or even monomer raw materials, has gained significant attentions.[14–16] Currently, non-catalytic pyrolysis is the primary chemical recycling technique for polyolefin plastics. However, this process has limited economic benefits due to the high reaction temperature and the low value of complex pyrolysis products.[17,18] In recent years, catalytic degradation has attracted increased attention as a viable process for the chemical recycling of polyolefin plastics under mild reaction conditions.[19,20] In previous studies, monofunctional catalysts such as ZSM-5 (ref. 21) and Hbeta[22] were employed for the cracking of polyolefin plastics, yielding substantial non-solid products. However, excessive low-value gas products were produced during the cracking process using the aforementioned monofunctional cracking catalysts.[23] Subsequently, bifunctional catalysts, such as Ru/HZSM-5,[24] MoS_x-Hbeta,[25] Pt/Beta,[26] Rh–

[a]College of Chemistry and Chemical Engineering, Institute for Sustainable Energy and Resources, Qingdao University, Qingdao 266071, Shandong, P. R. China. E-mail: duhui@qdu.edu.cn

[b]Liaoning Bora Bioenergy Co. Ltd, Panjin 124000, Liaoning, P. R. China

[c]College of Physics, Qingdao University, Qingdao 266071, Shandong, P. R. China

† Electronic supplementary information (ESI) available: Additional experimental details and materials as well as supporting data in including SEM, TEM, XPS and GCMS analysis used in this study. See DOI: https://doi.org/10.1039/d4ra02809k

Nb_2O_5,[27] *et al.*, offered both cracking and hydrogenation activities, have been reported for the catalytic degradation of polyolefin plastics. The polyolefin molecules were cleaved by the acidic sites of bifunctional catalysts *via* a carbocation reaction pathway, resulting in the generation of small molecular products.[28] Meanwhile, hydrogen was activated by the hydrogenation active sites, and the generated activated hydrogen would terminate the excessive cracking and condensation reaction. Therefore, the bifunctional catalysts were employed to cleave the inert C–C bonds of polyolefin at a manageable degree, facilitating the flexible and adjustable conversion of polyolefin plastics into liquid fuels with ideal carbon-chain lengths and excellent yields.[29–31] However, the previously reported bifunctional catalysts either employed noble metals through a complex preparation method or could only achieve low liquid products yield under high reaction temperature and pressure.[32–34]

Herein, we report noble metal-free nickel-based (Ni and NiS_2) bifunctional hydrocracking catalysts supported on Hbeta zeolites, demonstrating both acidic cracking and hydrogenation activities. The experimental results demonstrate that the acidic sites and suitable pore volume in Hbeta zeolites can effectively facilitate carbocation chain transfer reactions, thereby accelerate the generation of branched chains or ring products, which is beneficial to enhance the quality of liquid products. Moreover, the synergistic effect between Ni or NiS_2 and the acidic sites of Hbeta zeolites can significantly enhance the tandem cracking and hydrogenation of polyolefin plastics, which suppresses the formation of gas products and coke. By contrast, Ni-Hbeta show a better catalytic performance than NiS_2-Hbeta at low reaction temperature. Ni-Hbeta employed as a catalyst can effectively degradation high-density polyethylene (HDPE) into high value liquid and gas products with high yield of 94% under 523 K and 3 MPa H_2. Besides, the prepared catalysts also show excellent catalytic performance for waste low-purity polyolefin plastics with various additives.

Experimental

Chemicals

Nickel chloride and dichloromethane were purchased from Shanghai Macklin Biochemical Co., Ltd. Sulfur powder was purchased from Tianjin Guangcheng Chemical Reagent Co., Ltd. High-density polyethylene (HDPE) was purchased from Dongguan Kadar plastic raw materials Co., Ltd. Hbeta-25 zeolite ($SiO_2/Al_2O_3 = 25$; specific surface area: 662 $m^2\ g^{-1}$; major pore size: 0.56–0.75 nm) was purchased from Tianjin Nanhua Catalyst Co., Ltd.

Catalyst preparation

As depicted in Scheme 1, in a typical synthesis process, 2 g of Hbeta zeolite was mixed with 2.7 g of nickel chloride solution with a certain concentration, which was fully stirred for 1 hour. Then, the slurry was vacuum dried in a vacuum oven at 353 K for 3 hours. The dried solid powder was placed in a tube furnace and reduced at 873 K for 2 hours in 80 standard cubic centimeters per minute (sccm) 5% H_2/Ar flow. Finally, after the reduction was completed, the sample was cooled to room temperature and passivated by using a 5% O_2/Ar flow rate (80 sccm per min) in a tubular furnace for 20 minutes. The prepared catalyst is labeled as Ni-Hbeta. Additionally, the synthesized Ni-Hbeta catalyst was further transformed into NiS_2-Hbeta catalyst *via* a high temperature vulcanization process. In brief, 6 g sulfur powder was placed in the front zone of the double-temperature tube furnace (573 K), and 1 g Ni-Hbeta zeolite was placed in the back end (873 K). The vulcanization of Ni-Hbeta catalyst was carried out in the Ar flow (80 sccm min^{-1}) for 3 hours.

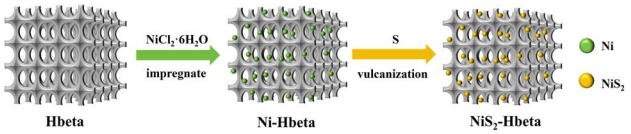

Scheme 1 Schematic illustration of the preparation process of Ni-Hbeta and NiS_2-Hbeta.

Catalyst characterization

X-ray diffraction (XRD) analysis of the synthesized catalysts was performed on a Bruker D8 Advance X-ray diffractometer using Cu Kα radiation (λ = 1.5418 Å) with 2θ = 10–80°. Chemical bonding states of the catalyst surfaces were characterized by X-ray photoelectron spectroscopy (XPS) measurements (XPS, Escalab 250Xi) with Al Kα radiation. Scanning electron microscopy (SEM) images were obtained using a Regulus 8100 apparatus on a sample powder previously dried and sputter-coated with a thin layer of gold. The morphology, size, and elemental mapping of the nano catalysts were observed by high-resolution transmission electron microscopy (HRTEM, FEI Tecnai G2 F20). The samples were dispersed in hexane by ultrasound, dropped on a copper grid, and observed at 200 kV.

Reaction tests and product analysis

Typically, the 25 ml autoclave reactor was sealed and filled with hydrogen to the target pressure to check the air tightness of the unit. Then, 2 g HDPE and 0.15 g catalyst (Ni-Hbeta or NiS_2-Hbeta) were placed in the reactor and sealed again. The autoclave reactor was purged with H_2 for 3 times and charged to 3 MPa H_2. The reactor was then slowly heated to 250 °C and maintained for 20 hours with a stirring speed of 800 rpm. After the reaction was completed, the reactor was quickly cooled to room temperature. For the post-consumer plastics, the samples were cut into small pieces and tested at the above conditions.

The gas products were collected using a gas sampling bag, while the rest non-gas products were rapid collected by a certain mass of dichloromethane at room temperature. Insoluble impurities and catalyst were then filtered, and 0.5 mL of filtrate was diluted with methylene chloride for liquid product selectivity analysis. The solution was detected on a gas chromatography mass spectrometer equipped with an HP-5MS UI column. The representative raw Gas Chromatography-Mass

Spectrometer (GCMS) data is shown in Fig. S1.† The data were analyzed using the "normalization method of peak area" to evaluate the selectivity of hydrocarbons. The filtered solid residue was dried in a vacuum oven at 353 K for 3 hours. The yield of the solid residue (Y_{solid}) was calculated gravimetrically, and the yield of the liquid products (Y_{liquid}) was calculated using the following eqn (1).

$$Y_{liquid} = \frac{m_{mixture} - m_{solid} - m_{catalyst} - m_{solvent}}{m_{initial}} \quad (1)$$

where $m_{mixture}$ is the mass of the unfiltered mixture, $m_{catalyst}$ is the mass of the catalyst, $m_{solvent}$ is the mass of methylene chloride, and $m_{initial}$ is the mass of the initial polymer feedstock.

The selectivity of product alkanes with i carbons (S_i) is evaluated from GCFID of liquid products. The selectivity of certain liquid products was calculated using the following eqn (2)

$$S_i = \frac{Y_i}{\Sigma_{liquid} Y_i} \quad (2)$$

where Y_i refers to the percentage of peak area occupied by hydrocarbons with carbon number i, and $\sum_{liquid} Y_i$ is the sum of the peak areas of all liquid products.

Results and discussion

To investigate the inherent distinctions between the catalysts, we used a variety of techniques to analyze Ni-Hbeta and NiS_2-Hbeta. The XRD results indicated that, when the zeolite's XRD peaks were subtracted, the XRD peaks of Ni-Hbeta and NiS_2-Hbeta can correspond to the standard cards with Ni (JCPDS 04-0850) and NiS_2 (JCPDS 89-1495). According to preliminary research, Ni-Hbeta and NiS_2-Hbeta exhibited high purity, and after being treated at a high temperature, the zeolite's crystal structure did not manifest any noticeable changes. This prevented zeolite and other impurities from interfering and made it easier to compare the differences in Ni and NiS_2's performances in the synergistic catalytic degradation of polyolefin plastics with Hbeta.

Then XPS was used to detect the chemical states and coordination environments of the main elements in Ni-Hbeta and NiS_2-Hbeta. It was clear from the lack of impurity peaks that Ni-Hbeta and NiS_2-Hbeta were exceptionally pure. In XPS, Ni and O were the main elements in the prepared catalysts (Fig. S2†), and S was the additional element in NiS_2-Hbeta. Where O was derived from nickel oxide produced by passivation process and Hbeta. Fig. 1B showed the high-resolution XPS spectrum of Ni 2p of Ni-Hbeta, with peaks located at 856.5 and 861.8 eV attributed to Ni $2p_{3/2}$ of Ni^{2+} and its satellite peaks, and the peak located at 853.1 eV attributed to the characteristic peak of Ni^0. The high-resolution XPS spectrum of Ni 2p of NiS_2-Hbeta was displayed in Fig. 1D. Peaks related to the Ni $2p_{3/2}$ peaks of Ni^{2+} and its satellites were situated at 853.9 and 861.8 eV, whereas peaks related to the Ni $2p_{3/2}$ peaks of Ni^{3+} were placed at 856.7 eV. A high degree of sulfidation was indicated by the spectra's lack of distinctive Ni^0 peaks. Ni^{2+} oxidation state was shown by the satellite peaks, while Ni^{3+} was the result of a minor oxidation of NiS_2-Hbeta. More research was done on sulfur's coordination environment and chemical state. Two prominent peaks at 163.5 and 162.6 eV were identified in the high-resolution XPS spectra of S 2p (Fig. 1C) and were ascribed to S $2p_{1/2}$ and S $2p_{3/2}$ of NiS_2, respectively.

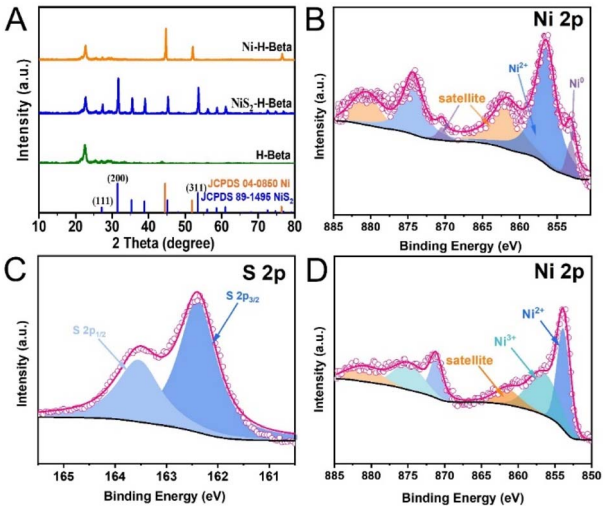

Fig. 1 (A) XRD patterns of the prepared catalysts and Hbeta; XPS spectra of (B) Ni-Hbeta and (C and D) NiS_2-Hbeta.

We next viewed the microscopic morphology of Ni-Hbeta and NiS_2-Hbeta by SEM. The morphology of Ni-Hbeta and NiS_2-Hbeta was irregular, and the size was basically the same, as seen in Fig. S3.† The results showed that the support of the prepared catalyst was highly consistent, which was convenient for the subsequent comparison of hydrogenation active centers. Furthermore, TEM was also used to examine the crystal structures and the distribution of Ni and NiS_2 on Hbeta. Nanoparticles adhered to the Hbeta zeolite edges were visible in the TEM pictures (Fig. 2A, D, S4 and S5†) of Ni-Hbeta and NiS_2-Hbeta. HRTEM image (Fig. 2B) of Ni-Hbeta showed distinct lattice striations attributed to the (111) crystallographic plane of Ni, indicating high crystallinity of Ni. HRTEM image (Fig. 2C) of NiS_2-Hbeta showed that the lattice spacing increased to 0.285 nm, which correspond to the (200) crystallographic plane of NiS_2. The catalysts were very pure, as evidenced by the EDS images (Fig. 2E and F) of Ni-Hbeta and NiS_2-Hbeta, which revealed that the elements Ni and S were equally spread on the Hbeta zeolites and that no other nucleating alloy structures existed.

Nowadays, catalysts play an increasing role in the degradation of pollutions[35–38] Using Hbeta-supported Ni-based catalysts (Ni-Hbeta or NiS_2-Hbeta), we examined the effects of reaction temperature and reaction duration on the co-catalytic degradation of polyolefin polymers. HDPE powder devoid of plasticizers, colorants, or other impurities was utilized as the reaction substrate in the evaluation experiments. We first evaluated the effect of reaction temperature (Fig. 3B and C). By utilizing Ni-Hbeta zeolite, with the increase of reaction temperature, the non-solid product yield shows a "stepwise" increase, while the

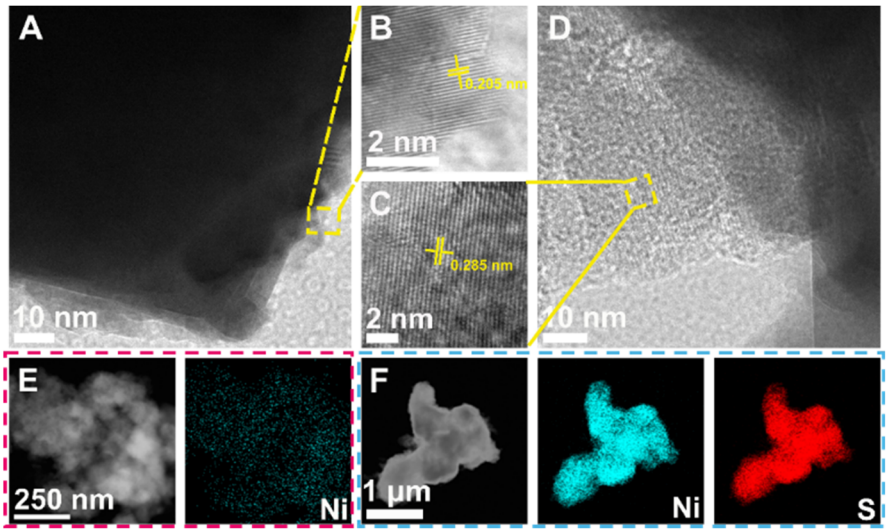

Fig. 2 TEM and HRTEM images of (A and B) Ni-Hbeta and (C and D) NiS_2-Hbeta. Corresponding EDS elemental mappings of (E) Ni-Hbeta and (F) NiS_2-Hbeta.

liquid yield shows a "volcano curve" that first increases and then decreases. By employing NiS_2-Hbeta zeolites, the total product yield increased with the increase of reaction temperature, while the liquid yield gradually decreased. It was easy to discover that activating the Hbeta zeolites' capacity to crack was hampered by too low a temperature, leading to the production of more solid residues. Additionally, an excessively high reaction temperature would cause polyolefin plastics to fracture excessively and arylation. Moreover, an excessively high reaction temperature would have two effects: it would increase the proportion of aromatics in the oil (>15%), making the fuel oil unusable for direct use, and cause high-quality alkanes (C5–C12) may excessively crack into lower-value short molecule gaseous hydrocarbons, lessening the economic return. Thus, it was found that 523 K was the ideal reaction temperature for both catalysts.

We further evaluated the effect of reaction time (Fig. 3D and E). For Ni-Hbeta zeolites, the non-solid yield and liquid yield gradually increased with increasing reaction time. For NiS_2-Hbeta zeolites, the non-solid yield gradually increased with increasing reaction time, while the liquid yield showed a small fluctuation. Overall, the increase in reaction time helped the liquid product distribution to be closer to the high-quality fuel oil. Therefore, the optimum reaction time for both catalysts was determined to be 20 hours.

The product distributions, in particular the cycloalkane and aromatic yields, were then analyzed for the prepared catalysts (Ni-Hbeta and NiS_2-Hbeta) and Hbeta at optimal reaction conditions (523 K, 20 h, 3 MPa) (Fig. 3A). Firstly, a distribution analysis of the product was conducted. When Hbeta zeolites were used in the reaction, the yields in liquid and gas phases were respectively 37% and 33%. The liquid yields rose to 78.6% and 64.3%, while the gas yields fell to 15.2% and 29.1%, respectively, with the addition of Ni-Hbeta and NiS_2-Hbeta. Iso paraffins made up the majority of the liquid products, and the percentage of premium fuel oil grew steadily (Hbeta < NiS_2-

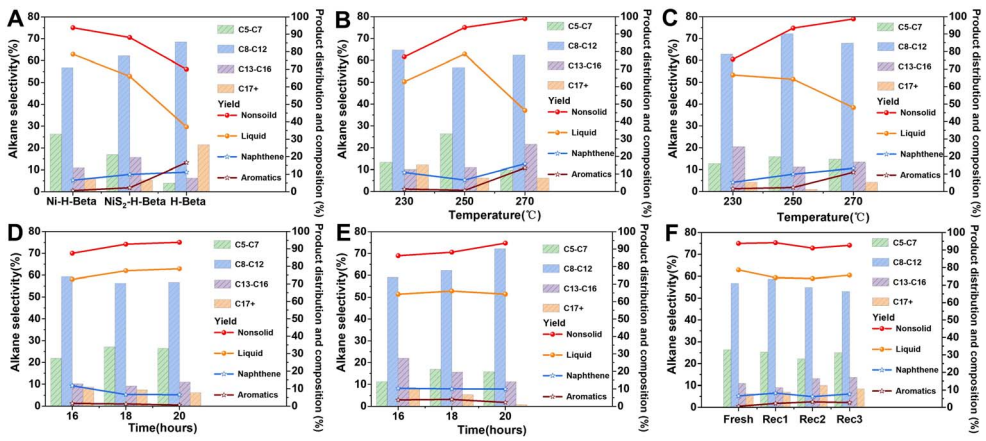

Fig. 3 (A) Comparison of different catalysts. (B and C) Influence of temperature (2 g of HDPE, 150 mg of catalyst, 20 hours, 3 MPa H_2). (D and E) Influence of time (2 g of HDPE, 150 mg of catalyst, 523 K, 3 MPa H_2). (F) Catalyst recyclability (2 g of HDPE, 150 mg of catalyst, 523 K, 3 MPa H_2, 20 hours). These values were calculated on carbon basis.

Hbeta < Ni-Hbeta). Next, the naphthenic and aromatic yields were further analyzed. The products of the blank control group had a higher percentage of aromatic and cycloalkane hydrocarbons. Notably, the yields of aromatic hydrocarbons appeared to drop dramatically while the yields of cycloalkanes declined more slowly when a metal active center (Ni or NiS_2) was added to the process. All things considered, the acidity of the Hbeta zeolites and the suitable pore volume can produce isomerization, and promote the transfer of carbon positive ion C–C chains to produce branched chains or rings, which can greatly improve the octane number. Additionally, the acidic nature of the sieves gives them a significant cleavage ability. However, the monofunctional Hbeta zeolites were unable to inhibit the condensation reaction accompanying the cleavage, resulting in the catalyst being prone to coking and deactivation. On the contrary, the introduction of metal active centers could rapidly adsorb, activate, and hydrogenate the unsaturated bonds generated by cracking into saturated alkanes, preventing the ring-forming and condensation reactions from proceeding, and facilitating the transfer of the carbon number distribution of the products to lighter alkanes. Combined with the results of XPS studies, it is easy to find that Ni^0 in Ni-Hbeta has a better hydrogenation activity at 523 K compared to Ni^{2+} in NiS_2-Hbeta, which is able to be more adapted to the cracking ability of Hbeta zeolite.

By closely studying the distribution of the reaction products, we were able to identify the co-catalytic reaction pathway. The acidic core of the carrier first breaks the polyolefin into carbon chain fragments with ethylene end groups. The metal active center near the pieces then absorbs and activates the hydrogen. The cyclization process is subsequently stopped when it combines with the ethylene end-groups that the carrier cleaves to form saturated alkanes. A tiny percentage of the aryl alkanes that were simultaneously generated under extreme pressure and heat were further adsorbed and hydrogenated by the metal-active sites to form cycloalkanes, yielding even higher-quality oil.

We also investigated the cyclic stability of Ni-Hbeta zeolites (Fig. 3F). To ensure the high activity of reduced nickel, the catalyst was reduced in a hydrogen-pressurized mixture at 773 K for two hours after each process. It was then passivated. There was no appreciable decrease in yield after four cycles, indicating the catalyst's strong stability.

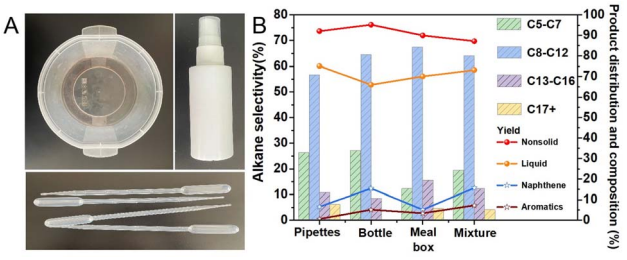

Fig. 4 Hydrocracking performance of real plastic wastes. (A) Illustration of different post-consumer polyethylene used in (B). (B) Catalytic performance of real polyethylene wastes (2 g of plastic, 150 mg of catalyst, 523 K, 3 MPa H_2, 20 hours).

Then we examined how well the catalyst degraded actual trash plastics (Fig. 4). Good liquid and non-solid yields were obtained when straws, lunch boxes, and bottles were broken up and exposed to the optimal reaction conditions, respectively. This demonstrated that the catalysts were unaffected by additives and other impurities. At last, the difficult-to-separate waste plastics can be directly converted into high-value oils and small molecule gases, skipping the sorting step, when the three waste plastics were mixed in equal proportions and reacted. The mixed polyolefin fragments were still able to achieve high liquid and non-solid yields under ideal reaction conditions.

Conclusions

In summary, two types of Ni-based catalysts supported on Hbeta zeolite, Ni-Hbeta and NiS_2-Hbeta, have been successfully synthesized for the hydrocracking of waste polyolefins. By incorporating of Ni or NiS_2 as hydrogenation cocatalysts onto the Hbeta zeolites, the synergistic effect between Ni or NiS_2 and the acidic sites of Hbeta zeolites can significantly enhance the tandem cracking and hydrogenation of polyolefin plastics, which suppresses the formation of gas products and coke. Moreover, Ni-Hbeta show better catalytic performances than NiS_2-Hbeta during the hydrocracking of HDPE at a relatively low temperature of 523 K. In particular, Ni-Hbeta employed as a catalyst can effectively degrade HDPE into high value liquid and gas products with high yield of 94% under 523 K and 3 MPa H_2, while also exhibiting excellent cycle stability. In addition, Ni-Hbeta exhibits a remarkable capability for efficient depolymerization of unsorted post-consumer polyolefin plastics (HDPE, LDPE, PP) containing various additives and pollutants. We believe the synthesized Ni-based catalysts supported on Hbeta zeolite have the potential to broaden the catalytic degradation of plastic waste and will serve as guidance for the design of noble metal-free and recyclable catalysts for achieving the circular economy of plastics.

Author contributions

GZ was involved in methodology, investigation, data curation, writing and original dra. YY helped in writing—original dra, conceptualization. QM contributed to conceptualization, methodology and data curation. RG contributed to methodology and data curation. YD contributed to methodology. HD contributed to writing – review & editing, supervision, resources and funding acquisition.

Conflicts of interest

There are no conflicts to declare.

Acknowledgements

The authors gratefully acknowledge the financial support from the National Natural Science Foundation of China (52172093, 21808115) and China Postdoctoral Science Foundation (2019T120571, 2018M632623).

Notes and references

1 R. Geyer, J. R. Jambeck and K. L. Law, *Sci. Adv.*, 2017, **3**, 0782.
2 V. Beghetto, R. Sole, C. Buranello, M. Al-Abkal and M. Facchin, *Materials*, 2021, **14**, 4782.
3 H. Sardon and A. P. Dove, *Science*, 2018, **360**, 380–381.
4 L. Yaqoob, T. Noor and N. Iqbal, *ACS Omega*, 2022, **7**, 13403–13435.
5 M. Li, Y. Pan, Z. Hou, Z. Wu, Z. Zeng and B. Wang, *Sci. Total Environ.*, 2023, **890**, 164359.
6 S. Ghosh, J. K. Sinha, S. Ghosh, K. Vashisth, S. Han and R. Bhaskar, *Sustainability*, 2023, **15**, 10821.
7 R. A. Muñoz Meneses, G. Cabrera-Papamija, F. Machuca-Martínez, L. A. Rodríguez, J. E. Diosa and E. Mosquera-Vargas, *Heliyon*, 2022, **8**, 9028.
8 E. Iacovidou, R. Geyer, J. Kalow, J. Palardy, J. Dunn, T. Hoellein, B. Xiong and E. Y. X. Chen, *One Earth*, 2021, **4**, 591–594.
9 C. Wang, H. Han, Y. Wu and D. Astruc, *Coord. Chem. Rev.*, 2022, **458**, 214422.
10 K. V. Khopade, S. H. Chikkali and N. Barsu, *Cell Rep. Phys. Sci.*, 2023, **4**, 101341.
11 J. E. Rorrer, C. Troyano-Valls, G. T. Beckham and Y. Román-Leshkov, *ACS Sustain. Chem. Eng.*, 2021, **9**, 11661–11666.
12 S. Wang, S. Ma, J. Qiu, A. Tian, Q. Li, X. Xu, B. Wang, N. Lu, Y. Liu and J. Zhu, *Green Chem.*, 2021, **23**, 2931–2937.
13 A. Thevenon and I. Vollmer, *Angew. Chem., Int. Ed.*, 2023, **62**, 6163.
14 T. Ibrahim, A. Ritacco, D. Nalley, O. F. Emon, Y. Liang and H. Sun, *Chem. Commun.*, 2024, **60**, 1361–1371.
15 L. Zou, R. Xu, H. Wang, Z. Wang, Y. Sun and M. Li, *Natl. Sci. Rev.*, 2023, **10**, nwad207.
16 K. Faust, P. Denifl and M. Hapke, *ChemCatChem*, 2023, **15**, 0310.
17 Q. Dai, H. Hu, C. Zou, Q. Gao, Y. Ren, X. Li, H. Liu, H. Liu and H. Yao, *Fuel*, 2024, **362**, 130825.
18 J. N. Hancock and J. E. Rorrer, *Appl. Catal., B*, 2023, **338**, 123071.
19 O. Akin, R. J. Varghese, A. Eschenbacher, J. Oenema, M. S. Abbas-Abadi, G. D. Stefanidis and K. M. Van Geem, *J. Anal. Appl. Pyrolysis*, 2023, **172**, 106036.
20 N. Netsch, J. Vogt, F. Richter, G. Straczewski, G. Mannebach, V. Fraaije, S. Tavakkol, S. Mihan and D. Stapf, *Chem. Ing. Tech.*, 2023, **95**, 1305–1313.
21 T. P. Paula, M. F. V. Marques and M. R. da Costa Marques, *J. Therm. Anal. Calorim.*, 2019, **138**, 3689–3699.
22 D. Munir, H. Amer, R. Aslam, M. Bououdina and M. R. Usman, *Mater. Renew. Sustain. Energy*, 2020, **9**, 9.
23 M. S. Abbas-Abadi, Y. Ureel, A. Eschenbacher, F. H. Vermeire, R. J. Varghese, J. Oenema, G. D. Stefanidis and K. M. Van Geem, *Prog. Energy Combust. Sci.*, 2023, **96**, 101046.
24 J. Du, L. Zeng, T. Yan, C. Wang, M. Wang, L. Luo, W. Wu, Z. Peng, H. Li and J. Zeng, *Nat. Nanotechnol.*, 2023, **18**, 772–779.
25 Z. Qiu, S. Lin, Z. Chen, A. Chen, Y. Zhou, X. Cao, Y. Wang and B.-L. Lin, *Sci. Adv.*, 2023, **9**, eadg5332.
26 C. A. A. Monteiro, D. Costa, J. L. Zotin and D. Cardoso, *Fuel*, 2015, **160**, 71–79.
27 B. Du, X. Chen, Y. Ling, T. Niu, W. Guan, J. Meng, H. Hu, C.-W. Tsang and C. Liang, *ChemSusChem*, 2023, **16**, 2035.
28 P. A. Kots, B. C. Vance and D. G. Vlachos, *React. Chem. Eng.*, 2022, **7**, 41–54.
29 L. Chen, J. B. Moreira, L. C. Meyer and J. Szanyi, *Appl. Catal., B*, 2023, **335**, 122897.
30 R. Chen, L. Cheng, J. Gu, H. Yuan and Y. Chen, *Energy Convers. Manage.*, 2024, **300**, 117983.
31 S. Rejman, I. Vollmer, M. J. Werny, E. T. C. Vogt, F. Meirer and B. M. Weckhuysen, *Chem. Sci.*, 2023, **14**, 10068–10080.
32 P. Zhao, W. Guo, Z. Gui, J. Jiang, Z. Zhu, J.-J. Li, L. Zhao, J. Zhou and Z. Xi, *ACS Sustain. Chem. Eng.*, 2024, **12**, 5738–5752.
33 Z. Chen, B. J. Erwin and L. Che, *J. Cleaner Prod.*, 2023, **424**, 138861.
34 A. A. Tedstone, A. Bin Jumah, E. Asuquo and A. A. Garforth, *Mater. Renew. Sustain. Energy*, 2022, **9**, 211353.
35 Z. Zhang, X. Zhan, B. Hong, X. Wang, P. Tang, Y. Ding, Y. Xia and Y. Zeng, *J. Colloid Interface Sci.*, 2024, **663**, 909–918.
36 Y. Zeng, Z. Zhang, X. Zhan, J. Xu, S. Liu, F. Wu, J. Li, B. Hong, X. Wang and Y. Xia, *Sep. Purif. Technol.*, 2024, **344**, 127211.
37 X. Zhan, Y. Zeng, J. Xu, Y. Xia, X. Wang, F. Tao, J. Ouyang, H. Li, L. Yang, S. Luo and B. Hong, *Chem. Eng. J.*, 2023, **464**, 142564.
38 Y. Zeng, X. Zhan, H. Li, X. Xiong, B. Hong, Y. Xia, Y. Ding and X. Wang, *Eur. Polym. J.*, 2023, **182**, 111734.